AGU PUBLICATIONS

JGR

Journal of Geophysical Research: Oceans

RESEARCH ARTICLE

10.1002/2015JC010894

Key Points:
- Polynya variability is examined using satellite-derived sea-ice data
- Ice production within a polynya balances the export of consolidated thin ice
- A simplified polynya model can represent the polynya variability well

Correspondence to:
K. Nakata,
kazuki-nakata@lowtem.hokudai.ac.jp

Citation:
Nakata, K., K. I. Ohshima, S. Nihashi, N. Kimura, and T. Tamura (2015), Variability and ice production budget in the Ross Ice Shelf Polynya based on a simplified polynya model and satellite observations, *J. Geophys. Res. Oceans*, *120*, 6234–6252, doi:10.1002/2015JC010894.

Received 8 APR 2015
Accepted 25 AUG 2015
Accepted article online 28 AUG 2015
Published online 15 SEP 2015

Variability and ice production budget in the Ross Ice Shelf Polynya based on a simplified polynya model and satellite observations

Kazuki Nakata[1], Kay I. Ohshima[2], Sohey Nihashi[3], Noriaki Kimura[4,5], and Takeshi Tamura[4,6,7]

[1]Graduate School of Environmental Science, Hokkaido University, Sapporo, Japan, [2]Institute of Low Temperature Science, Hokkaido University, Sapporo, Japan, [3]Department of Mechanical Engineering, National Institute of Technology, Tomakomai College, Tomakomai, Japan, [4]National Institute of Polar Research, Tachikawa, Japan, [5]Graduate School of Frontier Sciences, University of Tokyo, Kashiwa, Japan, [6]Department of Polar Science, Graduate University for Advanced Studies, Tachikawa, Japan, [7]Antarctic Climate and Ecosystems Cooperative Research Centre, University of Tasmania, Hobart, Tas, Australia

Abstract We examined to what degree a simplified polynya model can explain a real polynya based on satellite-derived sea-ice data. In the model, the polynya area, defined as the frazil ice production region, is determined by a balance between the offshore consolidated ice drift and frazil ice production. We used daily polynya area, ice production, and ice drift data derived from AMSR-E. The study area is the Ross Ice Shelf Polynya (RISP), which has the highest sea-ice production in the Southern Ocean. As a modification of the original model to apply the available satellite data set, we introduced the lag time by which produced frazil ice is transported and accumulated at the polynya edge. The model represents a half (48–60%) of the polynya variability when using a lag time of 1.5 days. The frazil ice collection depth at the polynya edge, a key parameter in the model, is estimated to be ~16 cm. The expansion of the RISP is achieved by ice divergence, and the contraction is achieved mostly by ice production. Both the wind and the remaining components (mainly regarded as the ocean current component) in the ice divergence are larger in the western part of the RISP, which explains the larger extent there. In the one-dimensional frame, assuming that the frazil ice produced within the RISP transforms into consolidated ice with a thickness of 16 cm, the frazil ice production ($\sim 1.7 \times 10^3$ m^2 d^{-1}) within the RISP approximately balances the export ($\sim 1.6 \times 10^3$ m^2 d^{-1}) of consolidated thin ice from the RISP edge.

1. Introduction

A feature of the sea-ice cover over coastal areas is the appearance of coastal polynyas (regions of thin ice or ice-free areas), which form by offshore wind and/or ocean current. Coastal polynyas are the sites of intensive heat loss to atmosphere and therefore are often regarded as ice production factories. In coastal polynyas, dense shelf water (DSW) is formed by cold and saline brine rejection due to high ice production [*Morales Maqueda et al*., 2004]. The DSW formed in Antarctic coastal polynyas is considered to be the main source of Antarctic bottom water (AABW). Therefore, Antarctic coastal polynyas have important roles in ocean thermohaline circulation and biogeochemical cycles such as the CO_2 exchange between the atmosphere and deep ocean [*Hoppema and Anderson*, 2007]. Moreover, the polynyas are important as biological "hot spots" for the ecosystem in the polar regions because of active biological primary production there [*Arrigo and van Dijken*, 2003].

Sea-ice production, dense water formation, and biological primary production within the coastal polynya are directly related to polynya extent. The factors determining polynya extent and variability have been investigated in many studies [e.g., *Lebedev*, 1968; *Pease*, 1987; *Ou*, 1988; *Darby et al*., 1995; *Gallée*, 1997; *Willmott et al*., 1997; *Biggs et al*., 2000]. *Pease* [1987] proposed a simplified polynya model by considering a balance between the offshore sea-ice drift and ice production within the polynya (see section 4 for the details). In this model, a coastal polynya is defined as the region of frazil ice production (referred to as frazil ice region in our paper), which is the area that is surrounded by consolidated ice and coastline. Then the model assumes that the frazil ice accumulates at the polynya edge and is finally transformed into consolidated ice, considering that frazil ice in the polynya moves offshore faster than consolidated ice. This model implicitly

assumes that frazil ice moves offshore with infinite velocity and instantaneously accumulates at the polynya edge. In reality, it takes time for frazil ice to accumulate at the polynya edge. *Ou* [1988] modified the *Pease*'s [1987] model into a more realistic model by considering this transit time of frazil ice. In these models, as a key parameter, an assumed constant thickness of frazil ice accumulating at the polynya edge is defined as "collection depth." These two polynya models have been the basis of subsequent many polynya models.

The *Pease* [1987] and its modified model [*Ou*, 1988] incorporate both the dynamic and thermodynamic processes of the polynya in a simple way. Although these models include the essence of polynya physics, their quantitative comparison with the real ocean has been difficult partly because sufficient spatial and temporal resolution data have been limited both for dynamical sea-ice drift data and thermodynamical ice production data. Therefore, few studies have made direct comparison of these models with the observations incorporating the temporal variation, although there have been some studies which applied these models to the real ocean through various assumptions, such that sea-ice drift is indirectly estimated from wind data [*Markus and Burns*, 1995; *Winsor and Björk*, 2000; *Krumpen et al*., 2011]. To what degree can the model explain a real polynya? If it is applicable, how should the model be modified, and what is a realistic value of the collection depth? Clarification of these issues could also be useful for the parameterization of coastal polynyas in large-scale numerical models.

Recent development of sea-ice remote sensing has greatly enhanced investigation of coastal polynyas. Particularly, satellite passive microwave radiometers have been great tools to observe polynyas globally every day, regardless of darkness, cloud cover, or water vapor in the atmosphere [*Markus et al*., 1998; *Martin et al*., 2004]. *Tamura et al*. [2007] developed an algorithm to detect thin ice regions (i.e., polynyas) and to estimate ice thickness in the Southern Ocean from Special Sensor Microwave Imager (SSM/I). Further, *Tamura et al*. [2008] extended this algorithm to cover mapping of sea-ice production for Antarctic coastal polynyas. Sea-ice drift has been estimated from satellite data using the maximum correlation method [*Kwok et al*., 1998; *Kimura*, 2004] and used for polynya studies [*Kwok*, 2005]. As such, nowadays it is possible to obtain temporally seamless data related to polynya activity, such as thin ice thickness, sea-ice production, and sea-ice drift, thanks to advances in the application of the passive microwave data to sea-ice studies.

Advanced Microwave Scanning Radiometer for EOS (AMSR-E) operated for the period June 2002 to October 2011 and the Advanced Microwave Scanning Radiometer 2 (AMSR2) instrument has been operational since August 2012. These AMSR series sensors can provide much finer spatial resolution than SSM/I sensors. AMSR sensors are capable of a ~6 km grid spacing at best. *Comiso et al*. [2011] and *Nihashi and Ohshima* [2015] have estimated thin ice thickness and ice production with this resolution from AMSR-E data. *Kimura and Wakatsuchi* [2011] examined sea-ice divergence distribution associated with the polynyas using the AMSR-E ice drift data. Based on the finer resolution AMSR-E data, *Kern and Aliani* [2011] examined the relationship between ice production and dense water formation in Terra Nova Bay, and *Drucker et al*. [2011] investigated the relationship between ice production and ice drift in the Ross Sea.

In these updated studies, AMSR-E provides ice thickness and ice production data with a spatial resolution of ~6.25 km [*Nihashi and Ohshima*, 2015] and sea-ice drift data with a resolution of ~37.5 km [*Kimura and Wakatsuchi*, 2011]. These resolutions are still insufficient for many polynyas to be resolved, because the polynya width usually ranges from a few to several tens of km. However, the Ross Ice Shelf Polynya (RISP), which is the largest coastal polynya in Antarctica, has a frazil and thin ice area of ~25,000 km^2 with a width of 20–100 km [*Martin et al*., 2007; *Tamura et al*., 2008]. Thus, the RISP is the most capable of being resolved by AMSR-E, both dynamically and thermodynamically. In this paper, we use the RISP for verification of the simple polynya model.

The RISP has the highest ice production among the Antarctic coastal polynyas [*Tamura et al*., 2008; *Nihashi and Ohshima*, 2015] and is a major formation area of DSW, which is a precursor to AABW [*Jacobs and Comiso*, 1989; *Martin et al*., 2007]. Therefore, the formation and variability of the RISP is directly related to AABW formation and its variability. Recently, it has been reported that the bottom water in the Ross Sea has gradually freshened [*Jacobs et al*., 2002; *Jacobs and Giulivi*, 2010]. Although the major cause of the freshening is considered to be an enhanced glacial ice melt upstream and/or an increase in precipitation in the Ross Sea [*Jacobs*, 2004; *Rintoul*, 2007; *Jacobs and Giulivi*, 2010], a decrease in sea-ice production in the RISP can also be a candidate [*Tamura et al*., 2008]. Given the influence of this polynya on the properties of bottom water, the interannual variability of the extent and ice production of the RISP have been examined by several studies [*Martin et al*., 2007; *Tamura et al*., 2008; *Kern*, 2009; *Comiso et al*., 2011; *Drucker et al*., 2011].

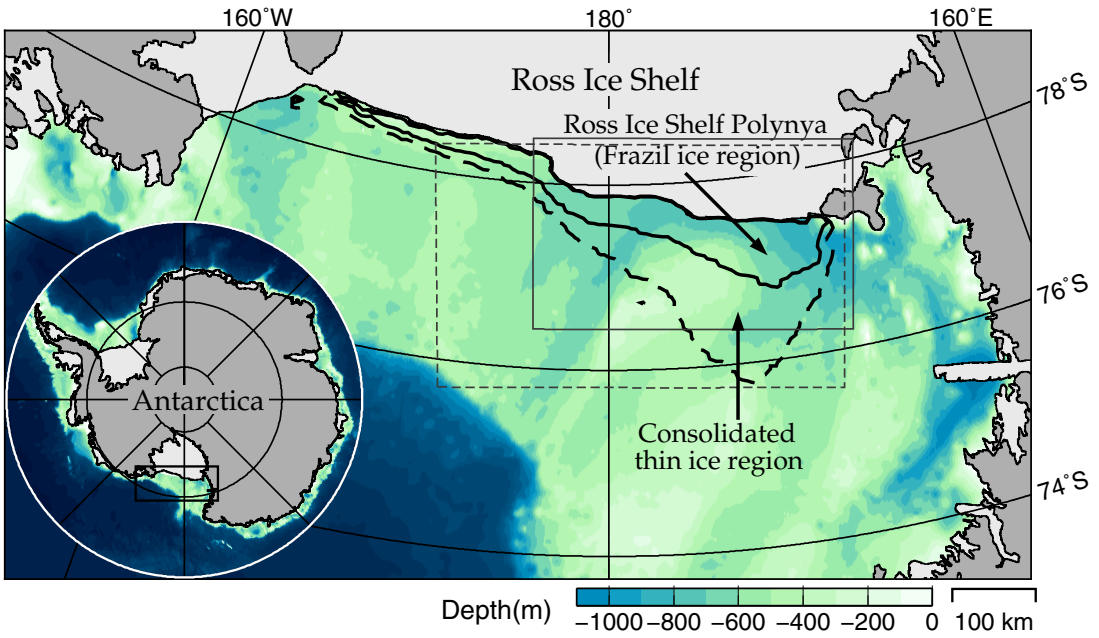

Figure 1. Bathymetry (color shading) of the Ross Sea and general locations of the Ross Ice Shelf Polynya (outlined by black solid lines) and consolidated thin ice region (outlined by black-dashed line), based on AMSR-E thin ice thickness data. The polynya and consolidated thin ice regions are defined as those with AMSR-E ice thicknesses of $\leq$12 and 12–20 cm, respectively (see sections 2 and 4 for details), and areas with appearance frequency of $>$15% are outlined. Thin solid and dashed boxes indicate the areas of Figures 9 and 10, respectively. The inset shows the entire Southern Ocean wherein a box denotes the enlarged portion.

This paper aims to reveal to what degree the simplified polynya model (*Pease* model) can represent the formation and variability of a real polynya, validated using the RISP. Specifically, using sea-ice thickness, production, and drift data from AMSR-E, we examine in detail the relationships between polynya area, ice divergence, and ice production. Investigation of the processes and variability of sea-ice production in the RISP will also enhance understanding the variability of AABW.

Figure 1 shows the distribution of the thin ice and frazil ice regions based on ice thickness data from AMSR-E, with the ETOPO1 bathymetry around the Ross Sea. In this paper, we define the frazil ice region as polynya, following the polynya model by *Pease* [1987]. In addition, we define the thin ice region extended just offshore of the polynya as consolidated thin ice region to distinguish from the frazil region and further offshore thick ice region.

This paper is structured as follows. Section 2 describes the data sets used in our analysis. Section 3 gives a general view of the RISP using the data sets. Section 4 describes the application method of the simplified model and gives the application result. In section 5, we quantitatively examine what determines the synoptic variability of the RISP. Section 6 discusses the validity of the simplified polynya model using Synthetic Aperture Radar (SAR) data, and the interannual variability of the RISP in the view of ice production budget. Section 7 gives our summary.

2. Data Description

All sea-ice data used in this study are derived from AMSR-E brightness temperatures, provided by the National Snow and Ice Data Center (NSIDC). We used sea-ice data for the period 2003–2010, from April to October when a large part of the Ross Sea is covered by sea ice.

For sea-ice thickness, we used daily thin ice ($\leq$20 cm) thickness data estimated from the AMSR-E algorithm developed by *Nihashi and Ohshima* [2015]. The thin ice thickness algorithm was based on comparisons between polarization ratio (*PR*) of AMSR-E brightness temperature and thermal ice thickness, which is obtained by heat flux calculation with sea-ice surface temperatures using MODerate resolution Imaging Spectroradiometer (MODIS) thermal infrared data. The thermal ice thickness is the one for which the calculated total heat flux using MODIS data would be realized under the assumption of uniform ice thickness in

the AMSR-E footprint [*Drucker et al.*, 2003; *Tamura et al.*, 2007]. Thus, the thermal ice thickness can be defined even in frazil ice regions. Thin ice thickness in the range of 1–10 cm is estimated from AMSR-E 89 GHz data (with a spatial resolution of ~6.25 km), and in the range of 10–20 cm thickness is estimated from 36 GHz data (spatial resolution of ~12.5 km). Daily ice thickness data are obtained from daily averaged brightness temperature data from both ascending and descending orbits.

Sea-ice production was estimated based on heat flux calculations using AMSR-E ice thickness, by assuming that heat from the ocean below is negligible and that all of the heat loss to the atmosphere goes toward freezing. The heat fluxes were calculated based on the formulae used in *Nihashi and Ohshima* [2001]. Heat loss to the atmosphere is calculated assuming that the sum of radiation and turbulent heat fluxes at the ice surface is balanced by the conductive heat flux in the sea ice whose thickness is derived from AMSR-E. Daily mean values of air temperature at 2 m, dew point temperature at 2 m, wind speed at 10 m, surface sea level pressure (SLP), and total cloud cover were used as atmospheric input data for heat flux calculations, from the 6 h ECMWF Interim Re-Analysis (ERA-Interim) data set (0000, 0600, 1200, and 1800 UT), with a spatial resolution of 0.5° × 0.5°. In addition, geostrophic winds calculated from the daily mean SLP fields were also used for the analysis in section 5.

Daily ice velocity was derived from AMSR-E data using the same procedure detailed in *Kimura and Wakatsuchi* [2011], based on the maximum cross-correlation method [*Ninnis et al.*, 1986; *Emery et al.*, 1991]. This method determines the spatial offset which maximizes the cross-correlation coefficient between two 89 GHz brightness temperature arrays (a spatial resolution of 6.25 km) in consecutive images, separated by 24 h. For the procedure, 6 × 6 pixel arrays are utilized, resulting in a drift data resolution of ~37.5 km. The grid points in which the correlation coefficient peak is 0.45 or less is treated as missing data. In addition, using a sea-ice concentration data set with a spatial resolution of 12.5 km from Enhanced NASA Team (NT2) algorithm provided by NSIDC, when a pixel with sea-ice concentration of <40% or the land pixel is included in the array, that array point is treated as a missing data point. In the calculation, points within 37.5 km from the coast, which may be affected by land contamination, are masked out. Therefore, ice drift within the polynya (frazil ice velocity) cannot be usually estimated in the data set because the width of the frazil ice region is generally less than 30 km (see section 6.3 for details). On the other hand, ice drift can be estimated in the consolidated thin ice region just off the polynya. This information is indispensable for examining polynya dynamics. The 89 GHz channel of AMSR-E tends to be affected by the water vapor and cloud. In such case, the ice drift is sometimes difficult to obtain, resulting in missing data. To prepare a seamless ice drift data set, we have also created the ice drift data using the 36 GHz channel data, which is much less hampered by water vapor. These 36 GHz data are substituted for the missing data in the 89 GHz data set.

Backscatter images acquired by the Advanced Synthetic Aperture Radar (ASAR: C-band SAR; the wavelength is 5.6 cm) on the European Space Agency's (ESA) Environmental Satellite (Envisat) were used for comparison and validation of the results of this study. The detailed sea-ice conditions can be seen from the SAR images with a high spatial resolution of ~150 m.

3. General View of the RISP

From the annual mean maps of thin ice coverage and sea-ice production (Figures 2a and 2b), a predominant thin ice region can be seen along the Ross Ice Shelf, with high sea-ice production. This large coastal polynya is formed by the dominant offshore sea-ice drift (Figure 2c), which is driven by an offshoreward wind, which forms due to a low-pressure system located in the eastern part of the Ross Sea [*Kwok*, 2005; *Kwok et al.*, 2007; *Petrelli et al.*, 2008; *Drucker et al.*, 2011]. Since the offshoreward ice drift dominates along the entire edge of the Ross Ice Shelf, the RISP has the largest length and area of all the Antarctic coastal polynya [*Drucker et al.*, 2011; *Nihashi and Ohshima*, 2015]. It is noted that the polynya extent is larger in the western part than in the eastern part (Figure 2a) because of faster ice drift in the western part.

Figure 2d shows the annual mean map of sea-ice divergence calculated from the ice drift data during April–October, indicating high ice divergence in the thin ice region along the Ross Ice Shelf. As described in section 2, most of the ice drift within the polynya is not detected, and ice drift in the offshore consolidated ice region is extrapolated into the grid cells inside the polynya. Thus, divergence near the Ross Ice Shelf implies divergence of the consolidated ice just outside of the polynya. Even from the climatological data, we can see the characteristics of the RISP, including the large size and high sea-ice production due to the high ice divergence caused by the offshoreward wind.

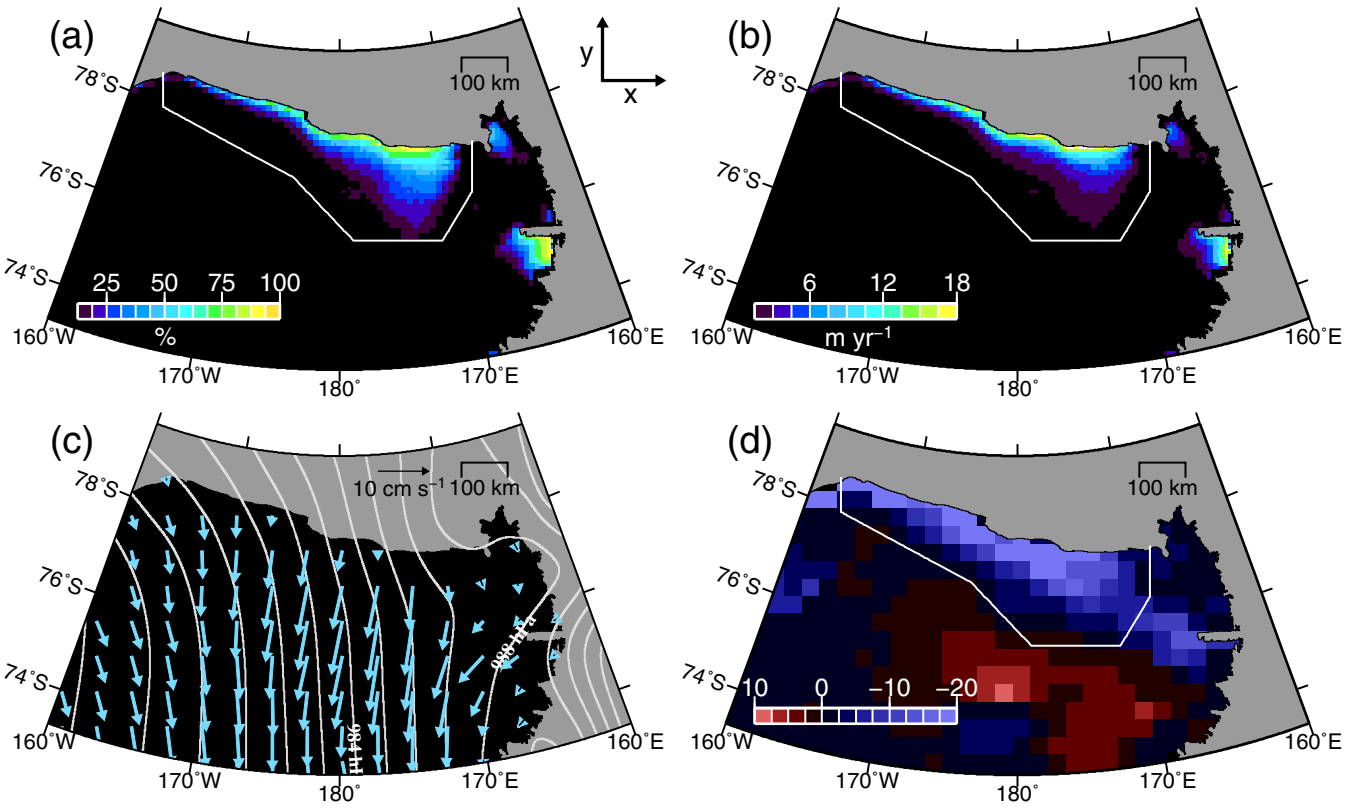

Figure 2. Maps of (a) frequency of occurrence (%) of regions with ice thickness of ≤20 cm, (b) annual cumulative sea-ice production (m yr^{-1}), (c) sea-ice motion (vector) and sea level pressure (contours), and (d) cumulative sea-ice divergence, during April–October averaged over the period 2003–2010. In Figure 2d, a value of 10.0, for example, corresponds to the 10 times area production during the freezing season in a year. The areas outlined by white in Figures 2a, 2b, and 2d are the calculation regions of section 4 for polynya area (*A*), ice production (*F*), and ice divergence (*DIV*), respectively.

In general, sea-ice drifts along the geostrophic wind [*Thorndike and Colony*, 1982]. Judging from the sea level pressure isobars and sea-ice drift in Figure 2c, this relationship is approximately satisfied in regions of >200–300 km from the Ross Ice Shelf (≲76°S). While the sea-ice drifts with an angle to the right of the geostrophic wind in regions of <200–300 km from the shelf (≳76°S). This region is located just off the RISP and is covered with relatively thin (but not frazil) ice (Figure 2a). The difference of the turning angle is probably due to the difference in ice conditions, particularly ice thickness [*Leppäranta*, 2005]. This suggestion from the climatological map will be discussed in detail in section 5.2.

4. Application of a Simplified Polynya Model to the RISP

4.1. A Simplified Polynya Model

First, we consider a one-dimensional polynya concept (Figure 3). A coastal polynya is formed by divergence of consolidated ice associated with offshore prevailing wind. Frazil ice produced in the polynya moves faster than the offshore consolidated ice, and thus the frazil ice is accumulated at the polynya edge and finally transformed into consolidated ice [*Pease*, 1987]. This process means that polynya extent is determined by a balance between divergence of consolidated ice and production of frazil ice. It is noted that it takes a time for the produced frazil ice to be transported and accumulate at the polynya edge. When we define frazil ice production rate in the polynya as *F*, offshore consolidated ice velocity as *DIV* and frazil ice volume in the polynya as *V*, the time variation of polynya width *dA*/*dt* can be expressed as follows [*Biggs et al.*, 2000]:

$$\frac{dA}{dt} = DIV - \frac{1}{H}\left(F - \frac{dV}{dt}\right), \tag{1}$$

where *H* is the collection depth (the thickness when frazil ice accumulates at the polynya edge). Assuming that frazil ice moves with infinite velocity and instantaneously accumulates at the polynya edge (i.e., $dV/dt = 0$), equation (1) can be reduced to the polynya model described by *Pease* [1987], which connects the dynamics

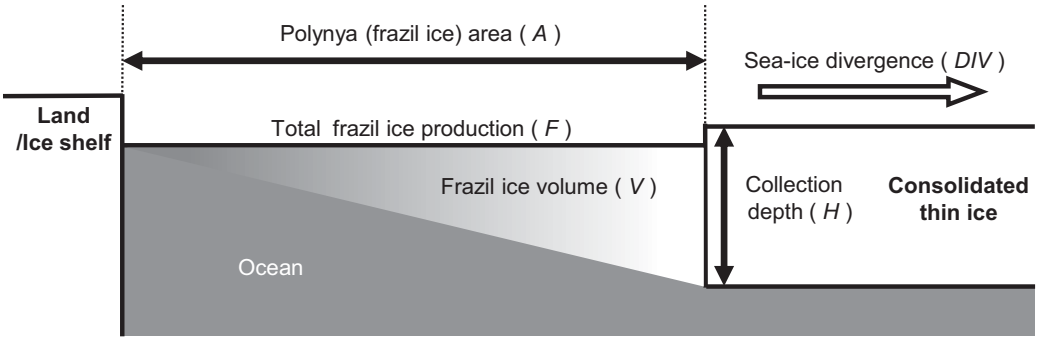

Figure 3. One-dimensional schematic of the polynya model described in equation (1).

and thermodynamics of the coastal polynya in the simplest way. *Ou* [1988] modified the *Pease* model by introducing the time scale of accumulation of produced frazil ice (i.e., $dV/dt \neq 0$). *Petrelli et al.* [2008] simulated the RISP extent using a coupled atmosphere-polynya model of *Gallée* [1997], which is based on the *Ou*'s [1988] model. Based on the available data set, we apply model 1 to the RISP, focusing on the following points. (i) To what degree can the simplified polynya model 1 represent the formation and variability of the RISP? (ii) What is the appropriate value of the collection depth *H*? (iii) How should we treat *dV*/*dt* in the analysis?

4.2. Method of Application

Here one-dimensional model 1 is extended two-dimensionally in our analysis. Specifically, we redefine *dA*/*dt* as variation of polynya area, *DIV* as sea-ice divergence, *F* as frazil ice production rate, and *V* as frazil ice volume integrated in polynya area, respectively. If both time series of the left and right sides of equation (1) can be calculated using available data sets, we are able to evaluate the model applicability by direct comparison. The time series of *dA*/*dt*, *DIV*, and *F* in equation (1) can be estimated from the daily data of AMSR-E thin ice thickness, ice production, and ice drift. However, we cannot directly obtain the frazil ice volume (*V*) and collection depth (*H*). The term *dV*/*dt* is related to the transport velocity of frazil ice and its accumulating time, which are hard to obtain. We therefore simplified equation (1), by introducing a typical time by which the produced frazil ice is transported and accumulated at the polynya edge, referred to as lag time τ (the detailed physical meaning of τ will be discussed in section 6.3), as follows:

$$\frac{dA(t)}{dt} = DIV(t) - \frac{F(t-\tau)}{H}. \tag{2}$$

In equation (2), unknown parameters are the collection depth *H* and lag time τ. In this study, we consider the balance of equation (2) for the area outlined by white in Figures 2a, 2b, and 2d (this analysis area is defined as the "box" hereinafter). Next we estimate the most suitable collection depth and lag time by least squares fitting for the time series of equation (2).

We define area with an AMSR-E-derived thickness of $\leq$12 cm as polynya and estimate the daily time series polynya area (*A*) by integrating all the area of grid cells detected as polynya in the box shown in Figure 2a (see section 4.4 for details of basis on the threshold value of 12 cm). Daily time series of polynya ice production (*F*) is estimated similarly for grid cells with an ice thickness of $\leq$12 cm in the box in Figure 2b. We also calculate daily time series of ice divergence in the RISP by integrating in the box in Figure 2d. At the polynya edge, which is located within about 100 km from the coast, sea ice predominantly moves offshore (Figure 2c). This offshore ice drift mostly determines the ice divergence of the polynya because of the zero flux at the coast. As shown in Figure 2a, the box is taken as a larger area than the polynya. Even so, considering that the ice divergence or convergence in the region between the polynya edge and the boundary of the box are much smaller than those of the polynya edge, sea-ice divergence in the box would be approximately determined by the divergence of the consolidated ice from the RISP edge. Since the sea-ice divergence in the box is determined by the normal flux of sea ice on the boundary of the box, according to Gauss' divergence theorem, the *DIV* would not depend on the extrapolation of ice drift data described in section 2.

We estimate each time series using a 2 day mean. The temporal grid of polynya area (*A*) and sea-ice production (*F*) correspond to that of the AMSR-E data. However, the temporal grid of *DIV* has a 0.5 day difference (lag) from that of *A* and *F*, because sea-ice drift is estimated from the difference of AMSR-E data of 2 days.

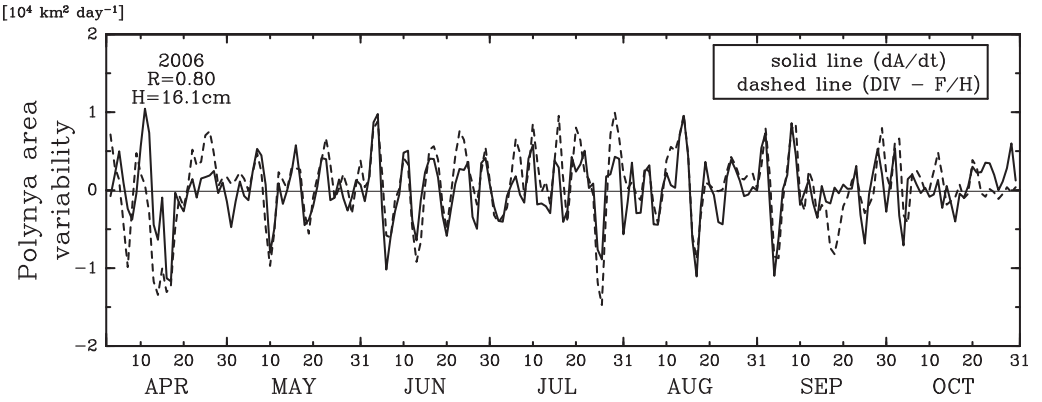

Figure 4. Time series of dA/dt (solid line) and $DIV-F/H$ (dashed line) in equation (1) during April–October 2006. Values of R and H in Figure 4 (top left) show the correlation coefficient between the two time series and the best-fitted collection depth, respectively.

Thus, considering this time lag for a time (t), with a 2 day average and $\tau = 0.5$ days, the terms dA/dt, DIV, and F in (2) are represented by $(A(t+1)-A(t-1))/2$, $(DIV(t+0.5)+DIV(t-0.5))/2$, and $(F(t)+F(t-1))/2$, respectively. Similarly, F with $\tau = 0$ corresponds to $(F(t-1)+F(t)\times 2+F(t+1))/4$, and F with $\tau = 1.5$ days corresponds to $(F(t-2)+F(t-1))/2$. Implications of the averaging will be discussed in section 4.4.

4.3. Results of the Application

Figure 4 shows time series of dA/dt and $(DIV-F/H)$ during April–October 2006, for the case of $\tau = 1.5$ days, $H = 16.1$ cm, and a 2 day mean. The polynya variability (dA/dt) corresponds very well with sea-ice divergence minus sea-ice production ($DIV-F/H$) with a high correlation coefficient of 0.80 (explained variance of ~64%). The average of correlation coefficients estimated for each year of 2003–2010 is 0.73, with a standard deviation of 0.04. These value means that even the simplest model 2 can represent a half (48–60%) of the RISP variability. Figure 4 shows the result in which the lag time τ is set to 1.5 days. If the lag time is not considered (i.e., $\tau = 0$), the correlation coefficient between dA/dt and $(DIV-F/H)$ is greatly reduced to 0.57 and root mean square error is 1.3 times as large as that in the case with $\tau = 1.5$ days. From our analysis using both the dynamic and thermodynamic time series data with relatively high resolution and accuracy, it is found that when the lag time is incorporated, the simplified model can better represent the polynya variability by ~20%, at least for the RISP. Further, this also suggests a possibility that polynya variability can be generally represented by the simplified model incorporating a typical lag time even if detailed information of frazil ice speed, whose in situ observation is quite difficult, cannot be obtained.

The 8 year average of the collection depth (H) estimated by least squares fitting each year is about 16 cm, with a standard deviation of only 1 cm. In previous model studies, the collection depth (H) is assumed to be 10 cm in *Pease* [1987], 20 cm in *Haarpaintner et al.* [2001], 10–30 cm in *Winsor and Björk* [2000], and 10 cm in *Morales Maqueda and Willmott* [2000]. So far, the collection depth has not been obtained based on statistically sufficient data. The collection depth estimated in our analysis using the long-term data is consistent with the assumed values in these past model studies.

Although all of the data in equation (2) are estimated from AMSR-E data, ice drift data (DIV) can be considered as independent data from polynya extent (A) and ice production data (F), since the calculation method of ice drift is completely different from those of the latter two. However, polynya extent and ice production data are dependent upon each other, because ice production is estimated from thin ice thickness data. From the view point of data independency, we should divide the terms of equation (2) into $(dA/dt+F/H)$ and DIV, and then examine their relationship. The 8 year average of correlation coefficient between them is calculated to be 0.67, which has a significance level of 99%. Although this value is lower than the value of 0.73 in the case of the main analysis between dA/dt and $DIV-F/H$, the apparent correlation by the data dependency between dA/dt and F/H in the main analysis is considered to be only in part.

4.4. Examination of the Setting

Figure 5 shows the lag correlation coefficient between F and dA/dt in the case of a 2 day mean, using a threshold ice thickness of 12 cm. The positive peak indicates an increase (decrease) of sea-ice production

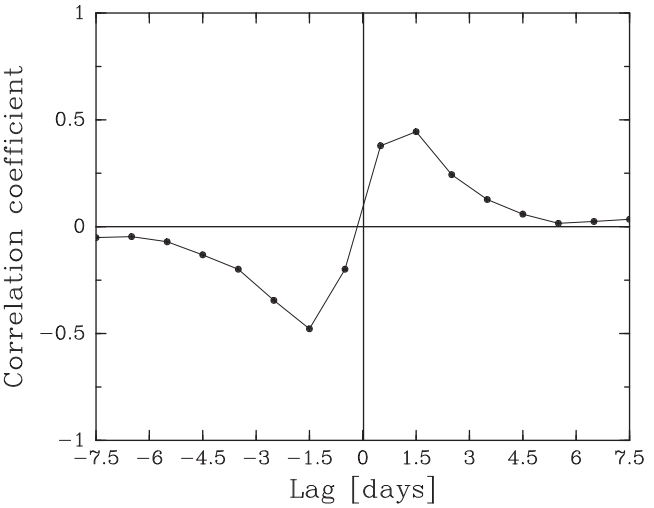

Figure 5. Lag correlation coefficient between sea-ice production (*F*) and rate of change of polynya area (*dA*/*dt*). A negative lag time implies that *F* leads *dA*/*dt*.

after a polynya expansion (contraction), and the negative peak indicates a polynya contraction (expansion) after an increase (decrease) of sea-ice production. The lag time in the latter peak is about 1.5 days, which partly rationalizes the setting of $\tau = 1.5$ days in Figure 4. Namely, this negative peak with the lag time indicates that it takes about 1.5 days on average for frazil ice in the RISP to be transported offshore and accumulated at the polynya edge. Further validation will be discussed in section 6.

The time series of Figure 4 and the main results in the previous section are based on a 2 day mean. The correlation coefficient between *dA*/*dt* and (*DIV*−*F*/*H*) using daily data without temporal averaging is 0.62, which is significantly lower than that (0.80) using a 2 day mean. In the cases of 3 and 4 day mean, the correlation coefficients are 0.70 and 0.67, respectively. The correlation coefficient is maximized in the case of a 2 day mean. For this dependency on the averaging procedure, the following two reasons are considered. One is that data errors are reduced by the mean operation. The other is that the process of movement and accumulation of frazil ice has an implicit role of low-pass filtering: Frazil ice accumulates at the polynya edge around the averaged rate of ice production for 2 days.

Figures 4 and 5 show the results with the threshold value of AMSR-E ice thickness set to 12 cm. Here we examine the dependency of the results on the threshold value of ice thickness. In model 2, the polynya is actually a frazil ice region. In reality, sea-ice thickness cannot be defined exactly in the frazil ice region. As mentioned in section 2, our thin ice thickness is the thermal ice thickness, for which the total heat loss can be calculated under the assumption of uniform ice thickness. As shown in *Drucker et al*. [2003], the frazil ice region, where ice and water is mixed, is detected by the satellite as a thin ice region with a thermal ice thickness of $<$10 cm. It is considered that increase in the fraction of frazil ice in seawater corresponds to the increases in thermal ice thickness. The threshold ice thickness should be selected as the thermal ice thickness where frazil ice is transformed into consolidated ice. Figure 6 shows the dependency of the correlation between *dA*/*dt* and (*DIV*−*F*/*H*) on the threshold value of AMSR-E ice thickness. The highest correlation occurs at a threshold thickness of 12 cm. By our interpretation, this implies that the transition from frazil ice to consolidated ice mostly occurs near 12 cm AMSR-E thickness. The highest correlation is the basis for the setting of the threshold ice thickness of 12 cm.

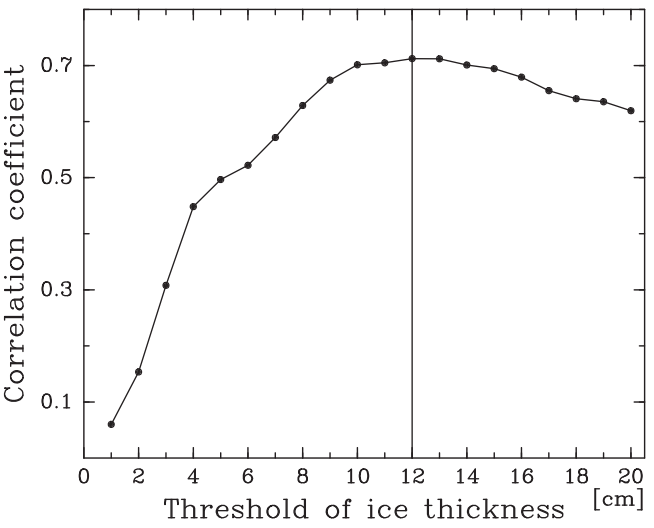

Figure 6. Correlation coefficients between *dA*/*dt* and *DIV*−*F*/*H* as a function of the threshold value of AMSR-E ice thickness for the polynya.

In this study, the regions of $\leq$12 cm AMSR-E thickness are regarded as the frazil ice region. However, under relatively calm conditions with a weak offshore wind, nilas should predominate rather than frazil ice. Such a situation is not identical to the *Pease* model represented by equation (2). Even in that situation, thin ice is finally transported

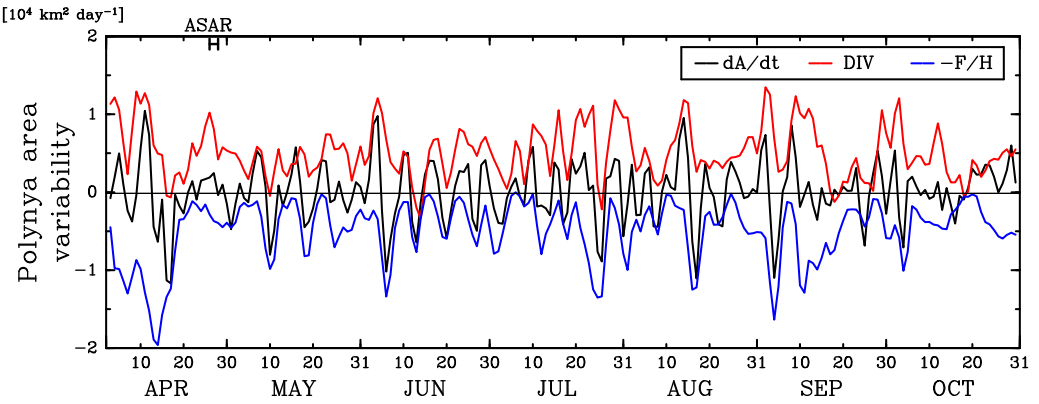

Figure 7. Time series of dA/dt (black line), dynamic term (DIV, red line), and thermodynamic term ($-F/H$, blue line) during April–October 2006. The marked period 25–27 April corresponds to ASAR time series in Figure 9.

offshore and accumulates into consolidated ice at the polynya edge when a strong offshore wind blows later. Good representation of the RISP variability by equation (2) indicates that the polynya concept by *Pease* [1987] is a good approximation in the RISP and that the frazil ice region roughly corresponds to the region of $\leq$12 cm AMSR-E thickness. This will be further supported by comparison and validation with SAR imagery in section 6.1.

Our analysis deals the collection depth (H) as a uniform value for 1 year to discuss the interannual variability in section 6. There is a way to estimate H such that the equation (2) is best fitted independently for each polynya event or the time scale of polynya variability, because the collection depth can be changed by the polynya area and other factors. We obtained a spectral peak at 7 or 8 days in the polynya variability. Thus, assuming the time scale of mean polynya event as 4 days, H is also calculated by the least squares fitting for all the 4 day segments. The 8 year average of the H for all the segments is about 15 cm, which is almost the same as that by 1 year least squares fitting. Also, the yearly averages of 8 years are almost the same. The fitting for a shorter period resultantly pushes the data error onto adjusting of H. We present H as a uniform value for each year in this paper, partly because the fitting for a longer period has a better statistically significance level.

5. Variability Factor of the RISP

5.1. Dynamics Versus Thermodynamics for Polynya Variability

In section 4, it is indicated that the simplified polynya model can represent the variability of the RISP well. The main external forces causing the polynya variability are considered to be wind and air temperature. In this subsection, we examine how the external forces determine the variability of the RISP dynamically and thermodynamically, using the time series data described in section 4.

Figure 7 shows time series of the dynamic term (DIV), the thermodynamic term ($-F/H$), and temporal change in the polynya area (dA/dt) in 2006. We can see the cycle such that the polynya expands during large ice divergent periods, and subsequently shrinks during high ice production periods, as in the period from early in June. To investigate the contributions of dynamic and thermodynamic terms to polynya variability, we calculate the correlation coefficients (R) and standardized partial regression coefficients (SPRC) between dA/dt and other terms for the entire period, the period of expansion ($dA/dt > 0$), and the period of contraction ($dA/dt < 0$) (Table 1).

Table 1. Correlation Coefficients (R) and Standardized Partial Regression Coefficients (SPRC) of dA/dt With DIV and $-F/H$, for the Freezing Season in 2003–2010

	DIV		$-F/H$	
	R	SPRC	R	SPRC
All	0.41	0.77	0.49	0.90
$dA/dt > 0$	0.50	1.20	−0.12	1.08
$dA/dt < 0$	0.07	0.96	0.67	1.48

For all time series data, dynamic and thermodynamic terms have comparable contribution to the polynya variability. However, when the polynya is expanding, the dynamic term has a higher correlation coefficient and

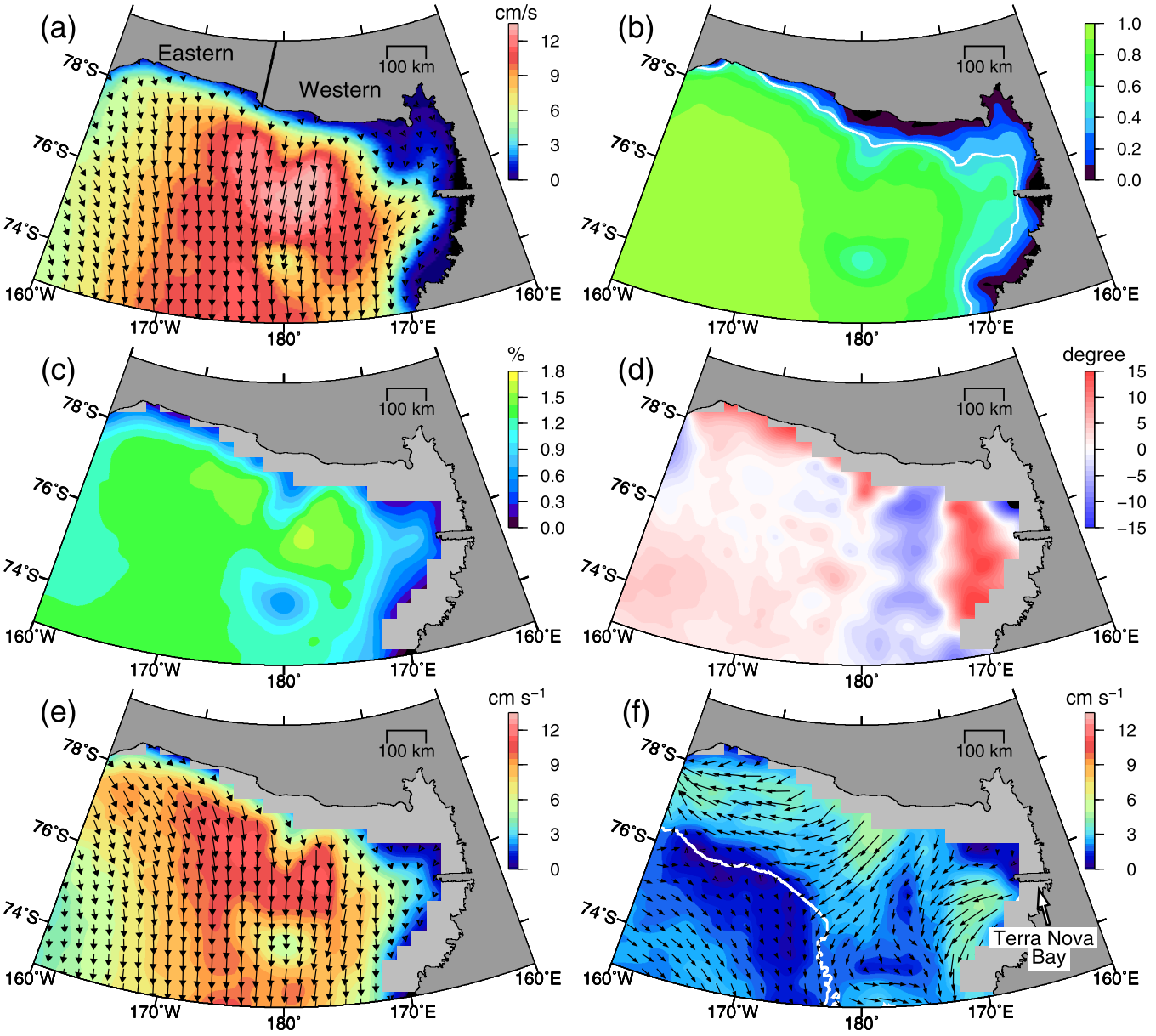

Figure 8. Maps of quantities of sea-ice drift for $dA/dt > 0$: (a) mean field of sea-ice motion, (b) correlation coefficient between wind and sea-ice drift, with the white contour showing a correlation coefficient of 0.4, (c) wind factor (%), (d) turning angle (degree), where leftward (rightward) ice drift relative to the wind direction is colored by red (blue), (e) wind component of sea-ice drift (cm s^{-1}), and (f) residual component of sea-ice drift (cm s^{-1}), with the white contour showing the location of the shelf break (1000 m depth). In Figures 8a, 8e, and 8f, the absolute speeds are represented by the color scale. The points with a correlation coefficient of <0.4 in Figure 8b are masked as light gray shading in Figures 8c–8f.

SPRC, while the thermodynamic term has no correlation with dA/dt. By contrast, when the polynya is contracting, the thermodynamic term has a higher correlation and SPRC, while the dynamic term has no correlation with dA/dt. These results demonstrate that expansion of the polynya is achieved dynamically through the ice divergence, while contraction is achieved thermodynamically mostly through sea-ice production. These results also show a small contribution of ice production decrease to the polynya expansion, and a small contribution of onshore ice drift to the polynya contraction.

5.2. Contribution of Wind and Ocean Components to Sea-Ice Divergence

The averaged field of sea-ice drift for $dA/dt > 0$ (Figure 8a) demonstrates that offshore ice drift predominates near the RISP. In general, sea-ice drift is mainly determined by wind. Thus, the sea-ice divergence at the polynya is considered to be caused mostly by wind. In this section, we precisely evaluate the

relationship between wind and sea-ice drift, in order to examine to what degree the wind determines the sea-ice drift or its divergence, and whether other factors (mainly ocean current) also contribute to the sea-ice drift or not. This analysis also leads to evaluation of the accuracy of the satellite-derived ice drift data.

Sea-ice motion on a time scale of 1 day or more is regarded as free drift in the case that internal ice stress is not large [*Thorndike and Colony*, 1982; *Leppäranta*, 2005]. In such a case, the sea-ice drift (U, V) can be written as,

$$\begin{pmatrix} U \\ V \end{pmatrix} = F \begin{pmatrix} cos\theta & -sin\theta \\ sin\theta & cos\theta \end{pmatrix} \begin{pmatrix} u \\ v \end{pmatrix} + \begin{pmatrix} \bar{c}_u \\ \bar{c}_v \end{pmatrix}, \tag{3}$$

where (u, v) is the geostrophic wind velocity, F is the wind factor (scaling factor between speeds of the wind and sea ice), θ is the turning angle of sea-ice drift for the wind, and $(\bar{c}_u, \bar{c}_v)$ is the constant residual term, which is mainly considered as the mean ocean current. The parameters (U, V), (u, v), and $(\bar{c}_u, \bar{c}_v)$ are aligned with the coordinate system of the polar stereographic grid where the abscissa and ordinate (x-y directions) are along the 90°E and 0°E meridians, respectively. First, we derived the turning angle and wind factor by applying the least squares method to equation (3) using the daily sea-ice drift and wind data for each grid cell. Further, we calculated correlation coefficient between (U, V) and (u, v), following the method by *Kimura* [2004]. Once the wind factor and turning angle can be obtained, the sea-ice drift can be divided into the wind and residual components from equation (3). Based on the map of each component, we examine how and to what degree sea-ice divergence is determined by the wind and ocean current.

We use 2 day means of dA/dt ($=(A(t+1)-A(t-1))/2$), sea-ice drift from AMSR-E, and geostrophic wind estimated from ERA-interim surface sea level pressure data, for the period 2003–2010. A 2 day mean is adopted because it can best represent the RISP variability in equation (2) (see section 4.2). Here we use the sea-ice drift data estimated only from 89 GHz channel data.

Figure 8b shows the map of correlation coefficient between the wind and sea-ice drift. No correlation in the region close to the Ross Ice Shelf is due to the lack of ice drift data. At the offshore region, which is presumed to be consolidated thin ice region, sea-ice drift corresponds to the geostrophic wind well with the correlation coefficient being more than 0.5.

The map of the wind factor (Figure 8c) shows that wind factor is around 1.3–1.7% in regions with a distance of $<$200–300 km from the coast while it decreases to 0.7–1.3% in the offshore region (distance $>$200–300 km). According to the map of turning angle (Figure 8d), a negative turning angle of $-7° \pm 6°$ (directed to the right of the geostrophic wind direction) is dominant in the western part of the offshore RISP, while a slight positive value of $3° \pm 3°$ is dominant in the eastern part. Considering that the surface wind is directed to the right of the geostrophic wind direction by $\sim$20° over the sea-ice region in the southern hemisphere [*Leppäranta*, 2005], the ice drift in the regions with negative turning angle is slightly (by 10–15°) directed leftward to the surface wind direction. This smaller value of turning angle is because in the thinner ice region the Coriolis (body) force becomes relatively small compared to the surface stress force by wind [*Kawaguchi et al.*, 2010]. Also from the analysis with 10 m surface wind of ERA-interim, it is confirmed that the turning angle in the western part is only slightly (by $10° \pm 5°$) directed to the left of the surface wind direction.

Now we examine the sea-ice divergence based on the spatial characteristics of the wind and residual components of the ice drift. Figure 8e shows the mean wind component of the ice drift (the first term of left hand side in equation (3)), estimated from the mean wind and the obtained wind factor and turning angle for $dA/dt > 0$. The offshoreward wind is predominant in the consolidated ice region offshore of the RISP, with a speed of $\sim$6 cm s^{-1} in the eastern part and $\sim$9 cm s^{-1} in the western part (see Figure 8a for the boundary of the western and eastern parts). The residual component of the ice drift (Figure 8f) shows clear spatial features: Larger offshore drift (3 cm s^{-1}) in the western part offshore of the RISP and slight offshore drift (1 cm s^{-1}) in the eastern part. We consider that the ocean current largely contributes to the residual component. These results suggest that the significant influence of the ocean current in the western part and that it partly explains the larger polynya extent and higher ice divergence in the western part (Figures 2b and 2d).

6. Discussion

6.1. Comparison With SAR Imagery

Our analysis is based on the simplified one-dimensional polynya concept shown in Figure 3, assuming that the frazil ice region is formed by ice divergence and the consolidated ice region is

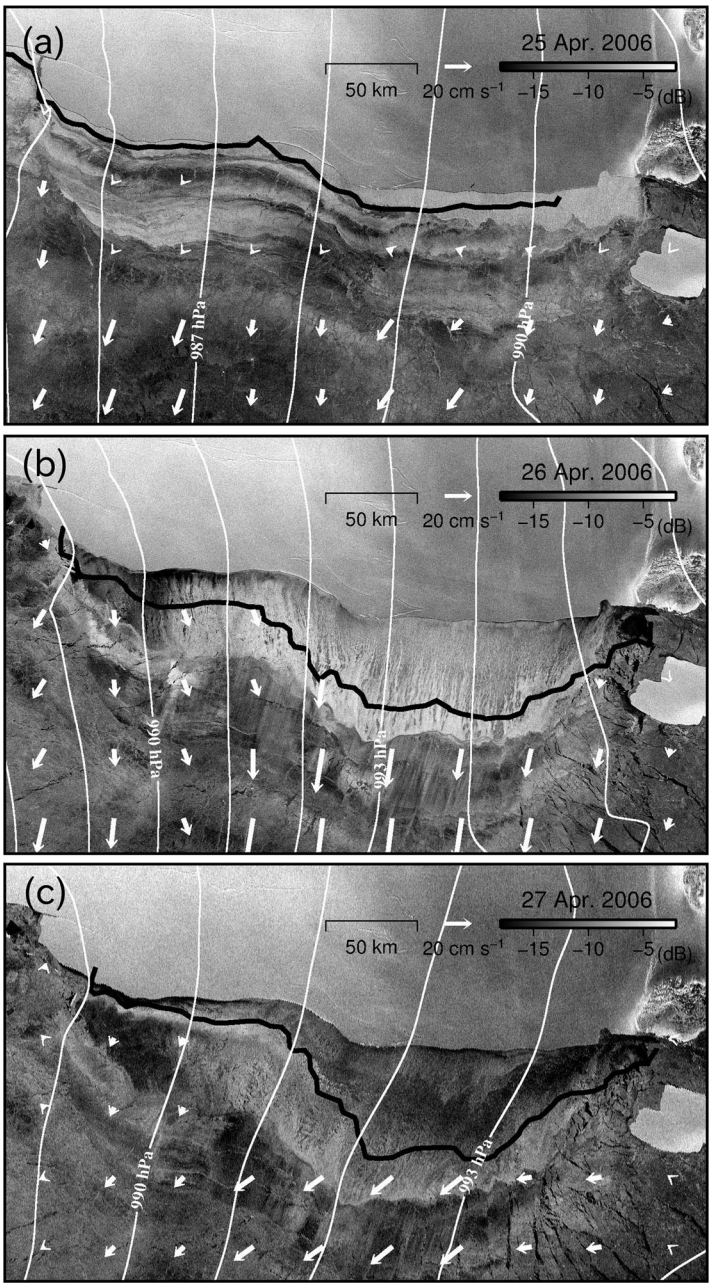

Figure 9. Envisat ASAR images on 25–27 April 2006. White vectors and contours show sea-ice drift and sea level pressure (contour intervals: 1 hPa) at the half-day before, respectively. Black lines show the threshold of 12 cm AMSR-E ice thickness. The black-white graded scale bar in the top right of each panel indicates the backscatter coefficient (dB).

subsequently formed by the accumulation of frazil ice. It is necessary to assess whether such concept is applicable to the RISP which actually has two-dimensional spatial extent and variability. However, it may be difficult to precisely identify the regions of frazil ice and consolidated ice from the AMSR-E data that can only provide the thermal ice thickness with the resolution of 6 km at best. Similarly, it is not confirmed whether the regions with $\leq$12 cm AMSR-E thickness correspond with frazil ice regions. To examine sea-ice conditions in the polynya at a high spatial resolution, regardless of atmospheric conditions, SAR is a powerful tool and has been used for some case studies of the RISP variability [*Kwok*, 2005; *Kwok et al*., 2007]. Especially, Envisat ASAR data with a resolution of about 150 m had been obtained all around Antarctica with relatively high frequency during the period 2002–2012 which covers the entire AMSR-E data set. Here we use ASAR data to examine the correspondence of the RISP to the simplified polynya model.

During the 2006 season, for which the time series is presented in section 4, sequential clear ASAR imagery of the RISP can be obtained only from 25 to 27 April, which is shown in Figure 9. In addition to the ASAR backscatter shown by the gray color scale, the contour of the 12 cm AMSR-E ice thickness threshold on the corresponding day, sea level pressure, and AMSR-E sea-ice drift at the half-day before are also shown in Figure 9.

We first examine the ASAR image on 26 April, when the polynya extent was largest in the 3 days. A high backscatter region with series of streaks extends 30–60 km just off the Ross Ice Shelf. The high backscatter streaks indicate long bands of active frazil ice approximately parallel to surface wind as in Langmuir circulation [*Drucker et al*., 2003]. It is found that the width of the streaks increase offshoreward, from several hundreds of meters to a few kilometers. Offshore of the streaks region, there is low backscatter region without streaks, which indicates a consolidated ice region. The contours of 12 cm AMSR-E ice thickness are located somewhat inshore from the boundary between the high and low backscatter regions. The streaks appear to merge and disappear around the region of 12 cm contours.

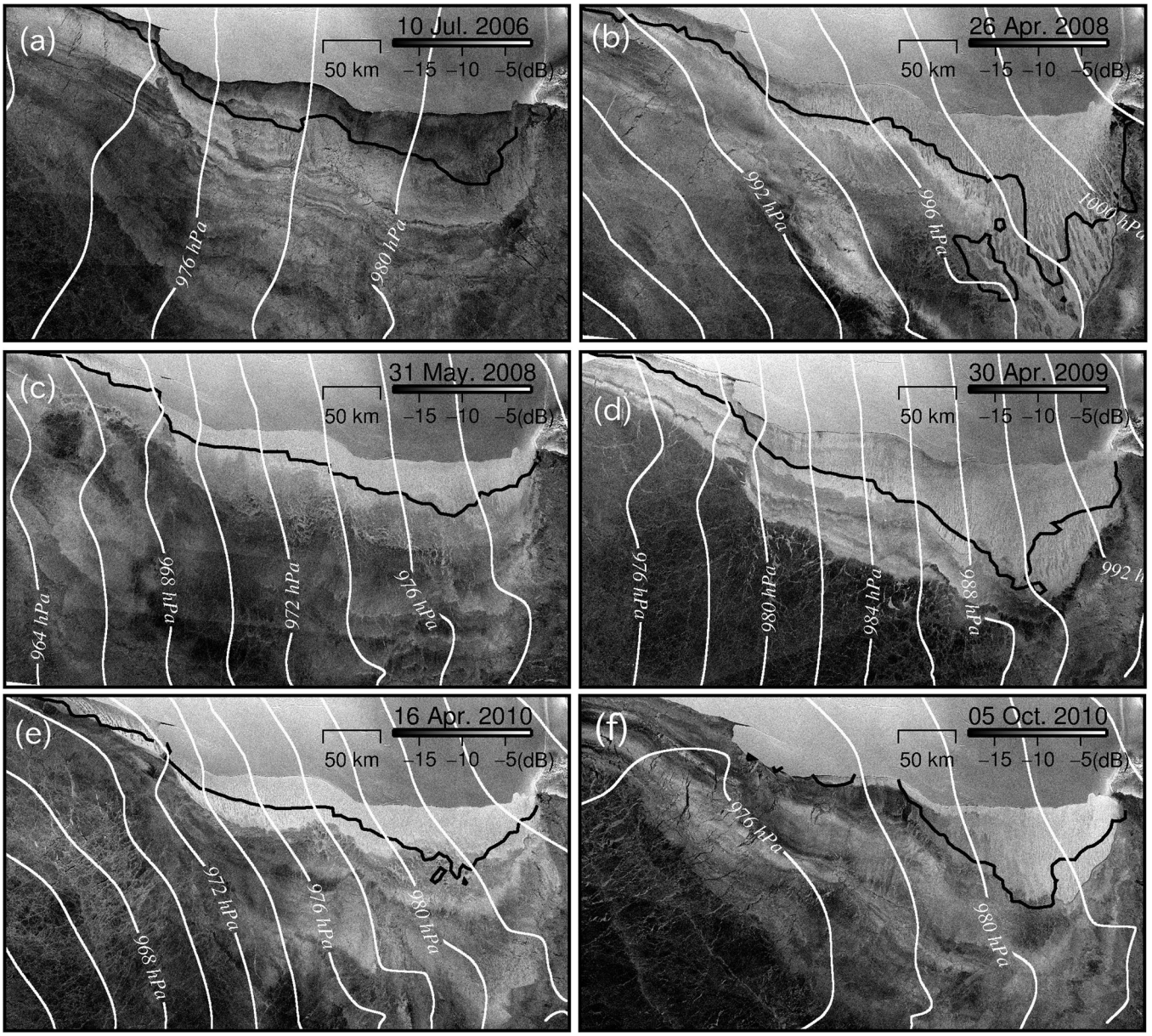

Figure 10. ASAR images on (a) 10 July 2006, (b) 26 April 2008, (c) 31 May 2008, (d) 30 April 2009, (e) 16 April 2010, and (f) 5 October 2010. Black and white lines show the 12 cm AMSR-E ice thickness threshold and sea level pressure (contour intervals: 2 hPa) on the corresponding day, respectively.

On 25 April 2006, the high backscatter region was still much smaller than that on 26 April, with the extent being less than 20 km. The polynya extends up to 60 km offshore during the 25–26 April due to large ice divergence caused by the offshore wind. This high backscatter region changed to a relatively low backscatter region on 27 April. This is probably because of relatively calm conditions with lower wind speed. The streak features are still visible in several places. Thus, the region is likely regarded as a frazil ice region. *Drucker et al*. [2003] also reported that the polynya could be a low backscatter region in SAR imagery, based on comparison with the mooring observations. By contrast, the high backscatter region just off this frazil ice region on 27 April shows the packed ice features with many ice floes and leads. The region is therefore considered to be consolidated new ice region formed by the accumulation of the frazil ice mainly produced on 26 April. The 12 cm AMSR-E ice thickness contour roughly corresponds to the boundary between these two regions. On 27 April, the offshore wind still continued but weakened, and a part of frazil ice within the polynya was likely transformed into consolidated thin ice, resulting in a plateau or contraction of the polynya area.

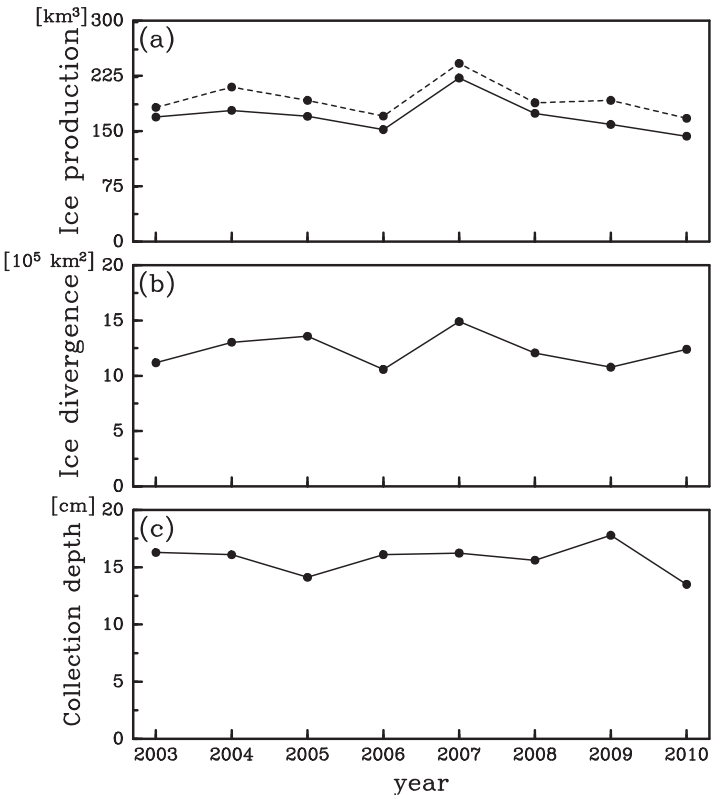

Figure 11. Interannual variability of (a) annual cumulative sea-ice production (*F*, solid line) with $DIV \times H$ (dashed line), (b) annual cumulative sea-ice divergence (*DIV*), and (c) averaged collection depth (*H*) during April–October for the period 2003–2010.

These features from the ASAR time series, roughly reflected in Figure 7, are consistent with the polynya concept of *Pease* [1987]. The frazil ice region is first extended due to prevailing offshoreward winds on 25–26 April (large *DIV* in Figure 7), resulting in an increase of frazil ice production (increase of *F*/*H* in Figure 7). Subsequently, the frazil ice is transformed into consolidated thin ice at the polynya edge on 27 April and finally the polynya area plateaus or contracts (change of *dA*/*dt* from positive to negative). It is noted that Figure 7 shows the result of a 2 day mean with inclusion of the eastern part of the RISP and thus does not exactly represent the ASAR time series (Figure 9) of the western part. Finally, the three ASAR images suggest that the contour of 12 cm AMSR-E ice thickness corresponds to the polynya edge to some extent.

We have actually compared 220 ASAR images with the corresponding map of AMSR-E ice thickness to examine whether the frazil ice region dominates in the RISP and the AMSR-E ice thickness of 12 cm corresponds to the polynya edge. Among these images, we present six more ASAR images which cover the whole RISP (Figure 10).

In these ASAR images, with the exception of Figure 10a, offshore winds are predominant and the high backscatter region with streaks appears just off the Ross Ice Shelf, which is considered to be the polynya (frazil ice) region. Especially in Figures 10b and 10d, the polynya has a width of about 100 km or more. On these 2 days, the contours of 12 cm AMSR-E ice thickness are located somewhat inshore from the boundary between the high and low backscatter regions, as in the ASAR image on 26 April 2006 (Figure 9b). On the other hand, the contours in Figures 10c, 10e, and 10f correspond well to the boundary. By contrast, in Figure 10a, a relatively low backscatter region appears off the Ross Ice Shelf under relatively low wind speed. A relatively high backscatter region exists just off this low backscatter region. These features are similar to those of the ASAR image on 27 April 2006 (Figure 9c). The backscatter features of the polynya strongly depend on the wind speed, due to surface wave generation. High offshore wind speed cases (Figure 10d) induce high backscattering and large extent of the polynya, and low wind speed cases (Figure 10a) induce low backscatter in the polynya. Figure 10 also supports the polynya concept of *Pease* [1987] and the AMSR-E thickness of 12 cm as the polynya edge to some extent. We admit that the exact evaluation is still difficult, even using ASAR.

6.2. Interannual Variability of the RISP

In this subsection, we discuss the interannual variability of total sea-ice production in the RISP (solid line in Figure 11a), on the basis of the polynya model concept described in section 4. The ice production presented in this study shows similar year-to-year relative variability to that of *Comiso et al*. [2011], although their absolute values are smaller mainly because of the different algorithm used. The interannual variability of the ice production corresponds well with that of total net ice divergence (Figure 11b) except in 2010, where the

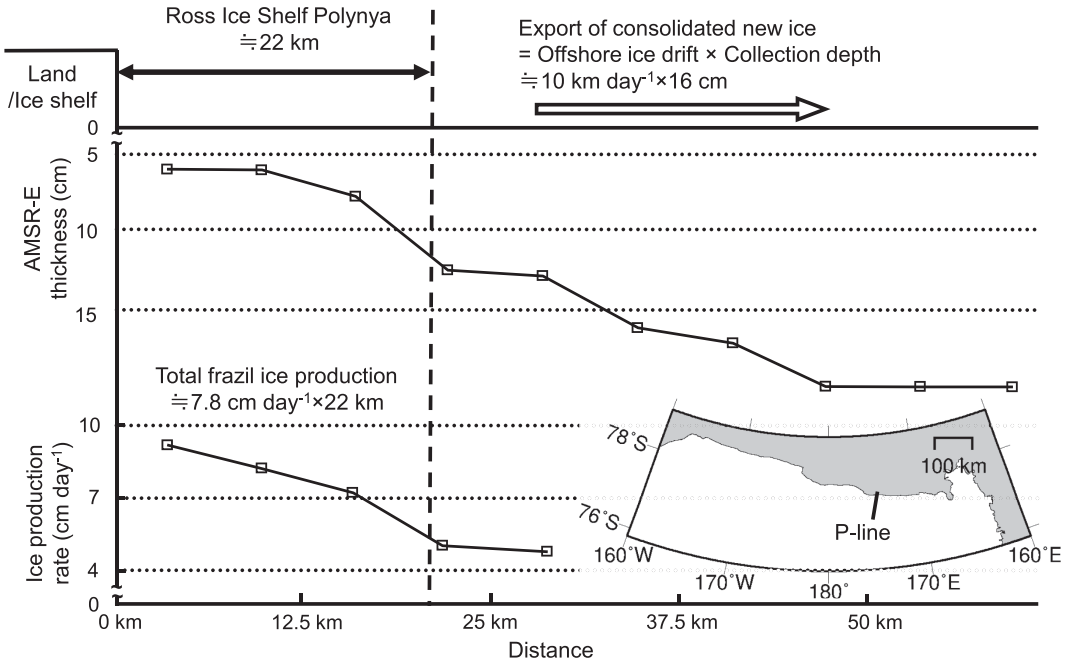

Figure 12. One-dimensional summary of sea-ice budget in the Ross Ice Shelf Polynya, deduced from AMSR-E data along the P-line indicated in the map in the bottom right.

correlation coefficient drops to 0.76. As a determining factor of the variability of sea-ice production, we also consider the yearly difference of averaged collection depth (Figure 11c), which is obtained by least squares fitting. It is noted that the collection depth of 2010 is the thinnest among the 8 years, which might explain the lowest ice production in 2010.

Here we consider a balance between ice production and ice divergence by incorporating the effect of collection depth. First, we assume that all of frazil ice produced within the polynya transforms into consolidated thin ice with a collection depth (H) throughout the year. Then, we can assume that the sum of these consolidated thin ices corresponds with the integration of the ice divergence (DIV) with an ice thickness of H. From this physical concept, the sum of ice production (F) should be equivalent to the sum of $DIV \times H$. We calculate the sum of $DIV \times H$ for each year and show its interannual variability (dashed line in Figure 11a). The sum of sea-ice production estimated by heat flux calculation using ice thickness and atmospheric data agrees very well with sum of the ice production estimated by multiplying ice divergence and collection depth (the correlation coefficient is 0.96), despite the fact that these two ice production values are estimated independently. This result is consistent with the proposed physical concept of $F = DIV \times H$; interannual variability of sea-ice production can be explained by considering both that of ice divergence and collection depth.

6.3. One-Dimensional Schematics of the RISP

Figure 12 shows the offshore variation of thermal ice thickness (represented by median), sea-ice production (by mean), and offshore ice drift (by mean) along the P-line (see right bottom of the figure), estimated using the AMSR-E data averaged over the period 2003–2010. The direction of the P-line is determined by the predominant direction of offshore ice drift. As shown in section 4.4, when the boundary of the polynya is defined as 12 cm AMSR-E ice thickness, the two time series (dA/dt and $DIV - F/H$) have the highest correlation. This implies that the boundary of the polynya or frazil ice region exists around 12 cm AMSR-E thickness on average. In Figure 12, it is shown that AMSR-E ice thickness along the P-line has a large gradient around the thickness of 12 cm, corresponding to 36 GHz polarization ratio $PR_{36} = 0.081$. This suggests that the microwave characteristics of sea ice significantly changes around the $PR_{36} = 0.081$. Consistently, the backscatter in the SAR images mostly changes around the $PR_{36} = 0.081$ (Figures 9 and 10). All these results rationalize the threshold thickness of 12 cm, which represents the boundary between frazil ice and consolidated ice regions. Although the thermal ice thickness may have errors arising from errors in atmospheric input data, such errors do not affect the fact that $PR_{36} = 0.081$ corresponds approximately to the polynya edge, and thus our results are not largely influenced by such errors.

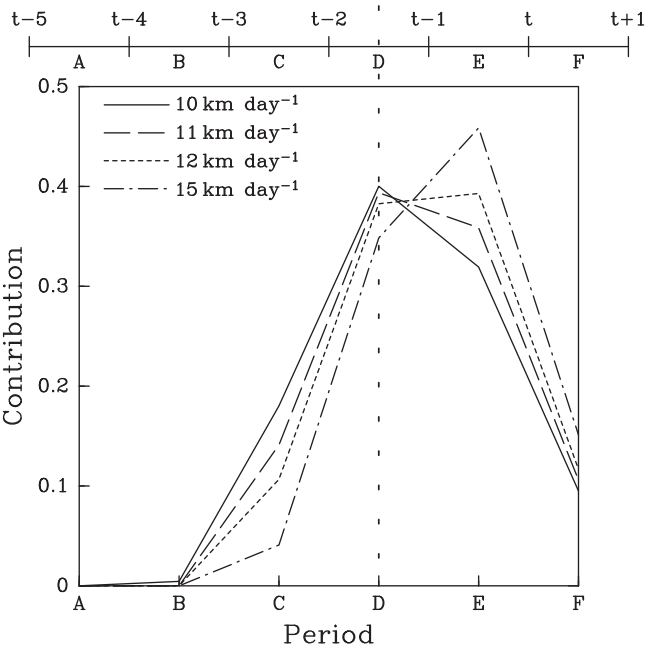

Figure 13. Amount of frazil ice originally produced in periods of A–F, accumulated at the polynya edge during the 2 days (from $t-1$ to $t+1$), for the cases of frazil ice velocity being 10, 11, 12, and 15 km d^{-1}.

When we assume that the turning angle difference between frazil and consolidated ice drifts is negligible, as in section 6.2, the relationship of $F=DIV\times H$ would be satisfied even in the one-dimension frame. The frazil ice production integrated over the frazil ice region of 22 km along the P-line per unit width (F) is calculated to be about 1.7×10^3 m^2 d^{-1}. The consolidated thin ice export from the polynya edge per unit width ($DIV \times H$) is calculated to be about 1.6×10^3 m^2 d^{-1} on average, when the 8 year average of collection depth (16 cm) is used. Namely, these comparable values suggest that $F=DIV\times H$ is satisfied to some extent even in the one-dimensional frame. The extent of the RISP is determined by a balance between frazil ice production and consolidated ice export, as schematically shown in Figure 12.

We here discuss the meaning of lag time obtained by a least squares fitting, based on the mean polynya features shown in Figure 12. First we assume that the RISP is in a steady state for simplicity, with the width being 22 km (mean value of the RISP). Then we assume that the frazil ice produced with the variation of sea-ice production rate shown in Figure 12 is transported offshore with the velocity comparable to or faster than the consolidated ice velocity ($\geq$10 m d^{-1}), and accumulated at the polynya edge and finally exported as consolidated thin ice. If we give the frazil ice velocity as an arbitrary value (10, 11, 12, and 15 km d^{-1}), we can estimate accumulation amount of original frazil ice produced in periods of A–E, at the polynya edge during the 2 days from $t-1$ to $t+1$ (Figure 13). We consider that the time in which the ice production becomes maximum for the accumulation corresponds to the lag time approximately. In Figure 13, a peak occurs at the period D, which corresponds to $\tau = 1.5$ days, in the cases of 10 and 11 km d^{-1}, while the peak moves to the period E in the case of 12 km d^{-1}. Namely, if the frazil ice velocity is assumed to be 10–12 km d^{-1} (frazil ice velocity is about 0–20% faster than the consolidated ice velocity), the lag time (τ) of 1.5 days consistently explains the sea-ice production budget for the mean RISP.

6.4. Effect of Oceanic Heat Flux

Jacobs and Comiso [1989] showed the existence of warm water mass at the ~78.1°S and 175.5°W and suggested the potential oceanic heat flux in excess of 100 W m^{-2}. Therefore, we may overestimate sea-ice production in the RISP. However, we consider that the total sea-ice production of the RISP is not largely influenced by the warm water because the warm water is only located off the eastern part of the RISP [*Orsi and Wiederwohl*, 2009], at which polynya width is not large. Since the series of SAR images (Figures 9 and 10) demonstrate active sea-ice production in the RISP, oceanic heat flux, even if it really occurs, is not large enough to prevent the sea-ice formation. Further, our analysis showed that the daily polynya variation is mostly determined by sea-ice production and divergence (Figure 4), and the offshore ice export well balance the ice production climatologically (Figures 11 and 12). These results, in turn, imply that the effect of the warm water on sea-ice production is not dominant in the RISP.

7. Conclusion

In this study, we have examined the applicability of the polynya model of *Pease* [1987], which connects the dynamic and thermodynamic processes of the polynya in the simplest way. Specifically, we have applied the model to the Ross Ice Shelf Polynya (RISP) using the high resolution sea-ice data recently created from

AMSR-E. We compared the time series of dA/dt (temporal change of polynya extent) estimated from thin ice data with that of DIV (ice divergence) minus F/H (ice production/collection depth) estimated from ice drift data and ice production data, respectively. As the model describes, the two time series well agree with each other, with a high correlation coefficient (the average value estimated in each year during 2003–2010 is 0.73). We conclude that even the simplest polynya model can represent a half (48–60%) of the polynya variability. For better representation of the polynya variability, the present study suggests incorporation of the lag time in which the frazil ice moves offshore and accumulates at the polynya edge (1.5 days in the case of the RISP). Good agreement between the model and observation in turn suggests the high reliability of the satellite-derived ice thickness, production, and drift data.

In our analysis, we can also estimate the collection depth of frazil ice (H), which is a key parameter in the model. The most suitable collection depth obtained by a least squares fitting is 16 ± 1 cm, which is consistent with the values assumed in the previous modeling studies. The fact that the two time series have the highest correlation when the threshold value of AMSR-E ice thickness is 12 cm implies that the transition from frazil ice to consolidated ice occurs at around 12 cm thermal ice thickness, corresponding to PR_{36} value of 0.081.

In most SAR images under an offshoreward wind, a region of a series of streaks, likely consisting of frazil ice, appears just off the Ross Ice Shelf, with the feature suggestive of accumulation of that frazil ice further offshore. These facts suggest the applicability and utility of the simplest polynya model proposed by *Pease* [1987]. The edge of the polynya (frazil ice region) shown in most of the SAR images roughly corresponds to the contour of 12 cm thermal ice thickness from AMSR-E. This rationalizes the choice of threshold value of 12 cm AMSR-E thickness as the polynya boundary in our analysis.

Based on the 2 day average data, we examined the contribution of the dynamic term (DIV) and thermodynamic term ($-F/H$) to the change in polynya area (dA/dt). The result shows that the extension of the polynya is determined by the ice divergence due to the offshore drift (dynamic term), while the retreat of the polynya is determined mostly by sea-ice production (thermodynamic term).

Next we investigated the cause of the sea-ice divergence, which determines the polynya extension. We partitioned the sea-ice drift into the wind component and the remaining component (mainly regarded as the ocean current component) and evaluated each contribution to the polynya extension. It is found that the major contributor is the wind component, with the remaining component contributing partly to the offshore drift, particularly in the western part of the RISP. This suggests the significant influence of the ocean current in the western part and explains the larger extension of the western part of the polynya than that of the eastern part.

In the one-dimensional frame, the extent and frazil ice production of the RISP are about 22 km and 1.7×10^3 m^2 d^{-1} on average, respectively. As expected, this frazil ice production approximately balances the export of consolidated thin ice from the polynya edge, estimated as 1.6×10^3 m^2 d^{-1}.

We could quantitatively evaluate the factors that determine the RISP variability to some extent. However, it should be noted that we could not consider the effects of the upwelling of warm Circumpolar Deep Water (CDW) [*Jacobs and Comiso*, 1989] and the calving of the Ross Ice Shelf [e.g., *Martin et al.*, 2007]. In the future, these effects should be addressed for comprehensive understanding of the RISP variability.

There are many coastal polynyas around Antarctica. It is interesting to examine whether or not the conceptual model used in our study is applicable to other polynyas. For most of other polynyas, the AMSR-E spatial resolution may be insufficient for the analysis due to smaller size of the polynyas. However, it is expected that similar analysis is possible in the Cape Darnley Polynya, which frequently extends up to 100 km offshore, and also in the Okhotsk Northwestern Polynya, which is the largest polynya in the northern hemisphere [*Nihashi et al.*, 2009]. The Cape Darnley Polynya has the second highest ice production in the Southern Ocean [*Tamura et al.*, 2008] and contributes to AABW formation [*Ohshima et al.*, 2013]. The Okhotsk Northwestern Polynya provides the source water for the North Pacific Intermediate Water [*Warner et al.*, 1996; *Shcherbina et al.*, 2003]. In that sense, the application of the model and analysis to these polynyas will be meaningful.

Acknowledgments
We acknowledge Alexander D. Fraser for his careful reading of the manuscript. We also thank Takenobu Toyota and Katsushi Iwamoto for their instructive comments. The AMSR-E brightness temperature and ice concentration data were provided by the National Snow and Ice Data Center (NSIDC), University of Colorado, Boulder, Colorado (http://nsidc.org/data/amsre/). The ECMWF ERA-interim data were obtained from the ECMWF data server (http://apps.ecmwf.int/datasets/data/interim-full-daily/). The Envisat ASAR data were provided by the European Space Agency (ESA) under the ESA project (ID 6130). Sea-ice data used for producing the results herein may be requested by contacting the authors. Sea-ice production data will be uploaded in the website (http://wwwod.lowtem.hokudai.ac.jp/polar-seaflux/). This work was supported by the fund from the Grant-in-Aids for Scientific Research (25241001 and 26740007) of the Japanese Ministry of Education, Culture, Sports, Science and Technology.

References

Arrigo, K. R., and G. L. van Dijken (2003), Phytoplankton dynamics within 37 Antarctic coastal polynya systems, *J. Geophys. Res.*, *108*(C8), 3271, doi:10.1029/2002JC001739.

Biggs, N. R. T., M. A. M. Maqueda, and A. J. Willmott (2000), Polynya flux model solutions incorporating a parameterization for the collection thickness of consolidated new ice, *J. Fluid Mech.*, *408*, 179–204, doi:10.1017/S0022112099007673.
Comiso, J. C., R. Kwok, S. Martin, and A. L. Gordon (2011), Variability and trends in sea ice extent and ice production in the Ross Sea, *J. Geophys. Res.*, *116*, C04021, doi:10.1029/2010JC006391.
Darby, M. S., A. J. Willmott, and T. A. Somerville (1995), On the influence of coastline orientation on the steady state width of a latent heat polynya, *J. Geophys. Res.*, *100*(C7), 13,625–13,633, doi:10.1029/95JC01024.
Drucker, R., S. Martin, and R. Moritz (2003), Observations of ice thickness and frazil ice in the St. Lawrence Island polynya from satellite imagery, upward looking sonar, and salinity/temperature moorings, *J. Geophys. Res.*, *108*(C5), 3149, doi:10.1029/2001JC001213.
Drucker, R., S. Martin, and R. Kwok (2011), Sea ice production and export from coastal polynyas in the Weddell and Ross Seas, *Geophys. Res. Lett.*, *38*, L17502, doi:10.1029/2011GL048668.
Emery, W. J., C. W. Fowler, J. Hawkins, and R. H. Preller (1991), Fram Strait satellite image-derived ice motions, *J. Geophys. Res.*, *96*(C3), 4751–4768, doi:10.1029/90JC02273.
Gallée, H. (1997), Air-sea interactions over Terra Nova Bay during winter: Simulation with a coupled atmosphere-polynya model, *J. Geophys. Res.*, *102*(D12), 13,835–13,849, doi:10.1029/96JD03098.
Haarpaintner, J., J.-C. Gascard, and P. M. Haugan (2001), Ice production and brine formation in Storfjorden, Svalbard, *J. Geophys. Res.*, *106*(C7), 14,001–14,013, doi:10.1029/1999JC000133.
Hoppema, M., and L. G. Anderson (2007), Biogeochemistry of polynyas and their role in sequestration of anthropogenic constituents, in *Polynyas: Windows Into Polar Oceans, Elsevier Oceanogr. Ser.*, vol. 74, edited by W. O. Smith and D. G. Barber, pp. 193–221, Elsevier, Amsterdam, doi:10.1016/S0422-9894(06)74006-5.
Jacobs, S. S. (2004), Bottom water production and its links with the thermohaline circulation, *Antarct. Sci.*, *16*(4), 427–437, doi:10.1017/S095410200400224X.
Jacobs, S. S., and J. C. Comiso (1989), Sea ice and oceanic processes on the Ross Sea continental shelf, *J. Geophys. Res.*, *94*(C12), 18,195–18,211, doi:10.1029/JC094iC12p18195.
Jacobs, S. S., and C. F. Giulivi (2010), Large multidecadal salinity trends near the Pacific–Antarctic continental margin, *J. Clim.*, *23*, 4508–4524, doi:10.1175/2010JCLI3284.1.
Jacobs, S. S., C. F. Giulivi, and P. A. Mele (2002), Freshening of the Ross Sea during the late 20th century, *Science*, *297*(5580), 386–389, doi:10.1126/science.1069574.
Kawaguchi, Y., S. Nihashi, H. Mitsudera, and K. I. Ohshima (2010), Formation mechanism of huge coastal polynyas and its application to Okhotsk northwestern polynya, *J. Phys. Oceanogr.*, *40*, 2451–2465, doi:10.1175/2010JPO4304.1.
Kern, S. (2009), Wintertime Antarctic coastal polynya area: 1992–2008, *Geophys. Res. Lett.*, *36*, L14501, doi:10.1029/2009GL038062.
Kern, S., and S. Aliani (2011), A comparison between polynya area and associated ice production with mooring-based measurements of temperature, salinity and currents in the southwestern Ross sea, Antarctica, *Ann. Glaciol.*, *52*, 291–300, doi:10.3189/172756411795931705.
Kimura, N. (2004), Sea ice motion in response to surface wind and ocean current in the Southern Ocean, *J. Meteorol. Soc. Jpn.*, *82*, 1223–1231, doi:10.2151/jmsj.2004.1223.
Kimura, N., and M. Wakatsuchi (2011), Large-scale processes governing the seasonal variability of the Antarctic sea ice, *Tellus, Ser. A*, *63*(4), 828–840, doi:10.1111/j.1600-0870.2011.00526.x.
Krumpen, T., et al. (2011), Sea ice production and water mass modification in the eastern Laptev Sea, *J. Geophys. Res.*, *116*, C05014, doi:10.1029/2010JC006545.
Kwok, R. (2005), Ross sea ice motion, area flux, and deformation, *J. Clim.*, *18*, 3759–3776, doi:10.1175/JCLI3507.1.
Kwok, R., A. Schweiger, D. A. Rothrock, S. Pang, and C. Kottmeier (1998), Sea ice motion from satellite passive microwave imagery assessed with ERS SAR and buoy motions, *J. Geophys. Res.*, *103*(C4), 8191–8214, doi:10.1029/97JC03334.
Kwok, R., J. C. Comiso, S. Martin, and R. Drucker (2007), Ross Sea polynyas: Response of ice concentration retrievals to large areas of thin ice, *J. Geophys. Res.*, *112*, C12012, doi:10.1029/2006JC003967.
Lebedev, V. L. (1968), Maximum size of a wind-generated lead during sea freezing, *Oceanology*, *8*, 313–318.
Leppäranta, M. (2005), *The Drift of Sea Ice*, 266 pp., Springer, N. Y.
Markus, T., and B. A. Burns (1995), A method to estimate subpixel-scale coastal polynyas with satellite passive microwave data, *J. Geophys. Res.*, *100*(C3), 4473–4487, doi:10.1029/94JC02278.
Markus, T., C. Kottmeier, and E. Fahrbach (1998), Ice formation in coastal polynyas in the Weddell Sea and their impact on oceanic salinity, in *Antarctic Sea Ice: Physical Processes, Interactions and Variability, Antarct. Res. Ser.*, vol. 74, edited by M. O. Jeffries, pp. 273–292, AGU, Washington, D. C.
Martin, S., R. Drucker, R. Kwok, and B. Holt (2004), Estimation of the thin ice thickness and heat flux for the Chukchi Sea Alaskan coast polynya from Special Sensor Microwave/Imager data, 1990–2001, *J. Geophys. Res.*, *109*, C10012, doi:10.1029/2004JC002428.
Martin, S., R. Drucker, and R. Kwok (2007), The areas and ice production of the western and central Ross Sea polynyas, 1992–2002, and their relation to the B-15 and C-19 iceberg events of 2000 and 2002, *J. Mar. Syst.*, *68*, 201–214, doi:10.1016/j.jmarsys.2006.11.008.
Morales Maqueda, M. A., and A. J. Willmott (2000), A two-dimensional time-dependent model of a wind-driven coastal polynya: Application to the St. Lawrence Island polynya, *J. Phys. Oceanogr.*, *30*, 1281–1304, doi:10.1175/1520-0485(2000)030<1281:ATDTDM>2.0.CO;2.
Morales Maqueda, M. A., A. J. Willmott, and N. R. T. Biggs (2004), Polynya dynamics: A review of observations and modeling, *Rev. Geophys.*, *42*, RG1004, doi:10.1029/2002RG000116.
Nihashi, S., and K. I. Ohshima (2001), Relationship between ice decay and solar heating through open water in the Antarctic sea ice zone, *J. Geophys. Res.*, *106*(C8), 16,767–16,782, doi:10.1029/2000JC000399.
Nihashi, S., and K. I. Ohshima (2015), Circumpolar mapping of Antarctic coastal polynyas and landfast sea ice: Relationship and variability, *J. Clim.*, *28*, 3650–3670, doi:10.1175/JCLI-D-14-00369.1.
Nihashi, S., K. I. Ohshima, T. Tamura, Y. Fukamachi, and S. Saitoh (2009), Thickness and production of sea ice in the Okhotsk Sea coastal polynyas from AMSR-E, *J. Geophys. Res.*, *114*, C10025, doi:10.1029/2008JC005222.
Ninnis, R. M., W. J. Emery, and M. J. Collins (1986), Automated extraction of pack ice motion from advanced very high resolution radiometer imagery, *J. Geophys. Res.*, *91*(C9), 10,725–10,734, doi:10.1029/JC091iC09p10725.
Ohshima, K. I., et al. (2013), Antarctic Bottom Water production by intense sea-ice formation in the Cape Darnley polynya, *Nat. Geosci.*, *6*, 235–240, doi:10.1038/NGEO1738.
Orsi, A. H., and C. L. Wiederwohl (2009), A recount of Ross Sea waters, *Deep Sea Res., Part II*, *56*, 778–795, doi:10.1016/j.dsr2.2008.10.033.
Ou, H. W. (1988), A time-dependent model of a coastal polynya, *J. Phys. Oceanogr.*, *18*, 584–590, doi:10.1175/1520-0485(1988)018<0584:ATDMOA>2.0.CO;2.

Pease, C. H. (1987), The size of wind-driven coastal polynyas, *J. Geophys. Res.*, *92*(C7), 7049–7059, doi:10.1029/JC092iC07p07049.
Petrelli, P., N. L. Bindoff, and A. Bergamasco (2008), The sea ice dynamics of Terra Nova Bay and Ross Ice Shelf Polynyas during a spring and winter simulation, *J. Geophys. Res.*, *113*, C09003, doi:10.1029/2006JC004048.
Rintoul, S. R. (2007), Rapid freshening of Antarctic Bottom Water formed in the Indian and Pacific oceans, *Geophys. Res. Lett.*, *34*, L06606, doi:10.1029/2006GL028550.
Shcherbina, A. Y., L. D. Talley, and D. L. Rudnick (2003), Direct observations of North Pacific ventilation: Brine rejection in the Okhotsk Sea, *Science*, *302*(5652), 1952–1955, doi:10.1126/science.1088692.
Tamura, T., K. I. Ohshima, T. Markus, D. J. Cavalieri, S. Nihashi, and N. Hirasawa (2007), Estimation of thin ice thickness and detection of fast ice from SSM/I data in the Antarctic Ocean, *J. Atmos. Oceanic Technol.*, *24*, 1757–1772, doi:10.1175/JTECH2113.1.
Tamura, T., K. I. Oshima, and S. Nihashi (2008), Mapping of sea ice production for Antarctic coastal polynyas, *Geophys. Res. Lett.*, *35*, L07606, doi:10.1029/2007GL032903.
Thorndike, A. S., and R. Colony (1982), Sea ice motion in response to geostrophic winds, *J. Geophys. Res.*, *87*(C8), 5845–5852, doi:10.1029/JC087iC08p05845.
Warner, M. J., J. L. Bullister, D. P. Wisegarver, R. H. Gammon, and R. F. Weiss (1996), Basin-wide distributions of chlorofluorocarbons CFC-11 and CFC-12 in the North Pacific: 1985–1989, *J. Geophys. Res.*, *101*(C9), 20,525–20,542, doi:10.1029/96JC01849.
Willmott, A. J., M. A. M. Maqueda, and M. S. Darby (1997), A model for the influence of wind and oceanic currents on the size of a steady-state latent heat coastal polynya, *J. Phys. Oceanogr.*, *27*, 2256–2275, doi:10.1175/1520-0485(1997)027<2256:AMFTIO>2.0.CO;2.
Winsor, P., and G. Björk (2000), Polynya activity in the Arctic Ocean from 1958 to 1997, *J. Geophys. Res.*, *105*(C4), 8789–8803, doi:10.1029/1999JC900305.